Simulation of electron dynamics subject to intense laser fields using a time-dependent Volkov basis

Cody Covington, Daniel Kidd, Justin Gilmer, and Kálmán Varga

Phys. Rev. A **95**, 013414 — Published 25 January 2017

DOI: 10.1103/PhysRevA.95.013414

Simulation of electron dynamics subject to intense laser fields using a time-dependent Volkov basis

Cody Covington, Daniel Kidd, Justin Gilmer, and Kálmán Varga*

Department of Physics and Astronomy, Vanderbilt University, Nashville, Tennessee 37235, USA

We present various intense laser-driven electron dynamics simulations performed using a Volkov basis set and compare results with other popular choices of basis. The Volkov basis is comprised of plane waves modified by a time-dependent phase factor, allowing for improved accuracy over other representations such as a real-space grid or plane wave basis. Alternatively, this advantage may be realized by being afforded significantly larger time step sizes in wave function propagation techniques. Comparisons of the Volkov basis set to other popular bases have been carried out for model one-dimensional finite and periodic systems as well as three-dimensional systems using time-dependent density functional theory, and the efficiency and accuracy of the Volkov approach have been demonstrated.

I. INTRODUCTION

Multiphoton ionization has been of great interest since the advent of lasers capable of generating intense electric fields [1–11]. This research has led to the discovery of a myriad of phenomena that take place when atoms and molecules are subjected to these fields [4, 10, 12, 13]. Interpretations of these experiments continue to take center stage as laser techniques advance to single cycle pulse durations and provide excellent temporal resolution for electron dynamics [14–18].

However, theoretical treatment of the electron-atom-laser interaction can be quite difficult. One may describe the strength of a laser by defining the Keldysh parameter [19] as $\gamma = \sqrt{I_P/2U_P}$, where I_P is the ionization potential, U_P is the classical ponderomotive energy given as $U_P = E_0^2/4\omega^2$, E_0 is the amplitude of the laser field, and ω is the angular frequency. Depending upon γ, there are typically three approaches: treat the laser as an external perturbation (weak laser, $\gamma >> 1$) [20], treat the atomic dynamics and laser field on equal footing ($\gamma \approx 1$), or assume the laser field is much stronger than the atomic/molecular potential [21–23] (strong laser, $\gamma << 1$).

To provide an accurate representation of the electron-laser interaction for moderate strength lasers, one must include both the atomic potential and external laser potential. However, the representation/localization of the time-dependent wave function in real-space is already problematic for a simulation involving ionization. When the electron wave function is exposed to the laser field, there will be some portion that tunnels away from the atoms and accelerates, as long as the laser is on, towards infinity. This will eventually result in part of the wave function hitting the boundary of the finite box or basis set it is confined to and cause the wavepacket to undergo reflections [24, 25]. If the boundary is not very far from the nuclei, this will lead to increased interaction with the center of the potential [24]. These interactions are artifacts resulting from the limitations of the current computational methods and are nonphysical in nature. To accurately capture the physical nature of the wave packet, a larger box must be used which is much more computationally taxing [24, 25].

Alternate methods have been implemented that, in return for yielding information about the electronic flux, allow for the calculation of more physical above threshold ionization spectra [10]. This has been accomplished by implementing electronic density sinks at the ends of the computational boundaries which are based on the type of information sought [26, 27]. An electron sink in the form of a complex absorbing potential (CAP) can be used; however, the parts of the wave function that pass into regions with a CAP are lost, and there is an additional drawback that the basis must be made larger to accommodate the CAP.

Another method for extending the simulation domain, known as the mask method or wave function splitting technique, is to divide the system into two regions: (A) a region treated quantum mechanically, usually via density functional theory (DFT), and (B) a region far from any nuclei, in which the Coulombic interactions with the nuclei and other electrons are negligible [10, 28–30]. This splitting of domains is advantageous due to the fact that in the absence of electron-nuclear and electron-electron interactions, the dynamics of a particle in an external time-dependent field may be described analytically using Volkov states, discussed below.

In this paper we will explore and test the applicability of Volkov states as time-dependent basis functions representing the wave functions in the entire computational domain. The Volkov states have been known for quite some time, but their application for multiphoton simulations has gone relatively unnoticed. They represent the exact solution to the time-dependent Schrödinger equation (TDSE) for a particle in a time-dependent electric field [31, 32]. Originally published by Collins and Merts, a procedure was composed to solve the three-dimensional (3D) TDSE by expanding the total system wave function

* kalman.varga@vanderbilt.edu

into a Volkov basis [32, 33]. The Volkov basis, although plane waves themselves, carry an additional phase factor that allows for a more accurate representation of the densities and other time-dependent properties compared to a pure plane wave basis.

As with any problem in quantum mechanics, the solution can usually be simplified by the correct choice of basis. Since the Volkov states are constructed with the purpose of satisfying the terms in the Hamiltonian attributed to the kinetic energy and external field, the Volkov state basis simplifies the TDSE and thus allows for a more accurate description of the response of electronic wave functions to strong external fields even when subject to an arbitrary external potential. Additionally, to solve the TDSE, efficient time evolution of the wave function is desirable and generally has large impact on the choice of basis [34–36].

The primary focus for this paper is to reiterate the simple formalism behind the Volkov basis propagation method and to provide a comparison with various methods that utilize time-independent bases including the finite difference (FD) method and the plane wave basis. Furthermore, the mask method is also evaluated and compared to Volkov and fully FD calculations which incorporate CAPs. A summary of the methods discussed in this paper is presented in table I.

II. FORMALISM

In this section, the Volkov state basis formalism is introduced for an arbitrary choice of potential and electric field, both of which may, in general, be time-dependent. Included are discussions of Volkov time propagation as well as the mask method. Atomic units (a.u.) are used throughout this paper.

A. Volkov states

Evolution of the electron wave function is governed by the TDSE, given as

$$i\frac{\partial\psi(\mathbf{r},t)}{\partial t} = H\psi(\mathbf{r},t). \tag{1}$$

The method of solution for this second order differential equation must be chosen carefully as it has a dramatic impact on the computational time required and the accuracy of the result. For the case of $H = T + V_1(t) + V_2(t) + \cdots$, one must consider the maximum rate of change among potential terms in order to determine the time step size necessary for accurate application of numerical integration schemes. Often when concerned with the effects of a strong laser, the field-electron interaction potential varies significantly faster than other terms. While removing the interaction entirely would neglect the physics one is interested in, it is possible to combine this term into a time-dependent basis.

The Volkov Hamiltonian describing the interaction of a free-electron with a laser field represented in velocity gauge is given by

$$H^V(t) = \frac{1}{2}\left(\mathbf{p} + \mathbf{A}(t)\right)^2. \tag{2}$$

In this case, the TDSE admits a solution as Volkov states

$$i\frac{\partial}{\partial t}\phi^V_{\mathbf{k}}(\mathbf{r},t) = H^V(t)\phi^V_{\mathbf{k}}(\mathbf{r},t), \tag{3}$$

where

$$\phi^V_{\mathbf{k}}(\mathbf{r},t) = e^{i\mathbf{k}\cdot\mathbf{r}}e^{-i\Phi^{\mathbf{k}}(t)}. \tag{4}$$

The time-dependent Volkov phase is defined as

$$\Phi^{\mathbf{k}}(t) = \int_0^t \frac{1}{2}\left(\mathbf{k} + \mathbf{A}(\tau)\right)^2 d\tau. \tag{5}$$

B. Time-dependent basis functions

The TDSE is most often solved by time propagating the wave function. In time propagation schemes, the wave function is expanded in a suitable basis

$$\psi(\mathbf{r},t) = \sum_{\mathbf{k}} c_{\mathbf{k}}(t)\phi_{\mathbf{k}}(\mathbf{r}), \tag{6}$$

where the basis functions are typically time-independent. By substituting this ansatz into the TDSE, one obtains

$$\sum_{\mathbf{k}}\left(i\dot{c}_{\mathbf{k}} - c_{\mathbf{k}}H\right)\phi_{\mathbf{k}}(\mathbf{r}) = 0. \tag{7}$$

In this approach, the full Hamiltonian matrix elements must be available, and accuracy is governed by choice of numerical time propagation method as well as the basis functions themselves.

Here, the wave function is instead expanded in terms of time-dependent basis functions $\phi_{\mathbf{k}}(\mathbf{r},t)$,

$$\psi(\mathbf{r},t) = \sum_{\mathbf{k}} c_{\mathbf{k}}(t)\phi_{\mathbf{k}}(\mathbf{r},t), \tag{8}$$

where we assume that the expansion coefficients are time-dependent as well. In ref. [11] it was shown that allowing time-dependence of both the coefficients and basis functions greatly enhances the flexibility of the expansion. By substituting this ansatz into the TDSE, one has

$$i\sum_{\mathbf{k}}\left(\dot{c}_{\mathbf{k}}\phi_{\mathbf{k}}(\mathbf{r},t) + c_{\mathbf{k}}\dot{\phi}_{\mathbf{k}}(\mathbf{r},t)\right) = \sum_{\mathbf{k}} c_{\mathbf{k}}H\phi_{\mathbf{k}}(\mathbf{r},t). \tag{9}$$

The Hamiltonian may now be separated into two parts, $H = H^V + V(t)$. By choosing the Volkov states as a basis, one may take advantage of the property $i\dot{\phi}^V_{\mathbf{k}} = H^V\phi^V_{\mathbf{k}}$ in order to obtain

$$\sum_{\mathbf{k}}\left(i\dot{c}_{\mathbf{k}} - c_{\mathbf{k}}V(t)\right)\phi_{\mathbf{k}}(\mathbf{r},t) = 0. \tag{10}$$

TABLE I. Summary of the various method compared to the Volkov approach throughout this paper. Note that while the Volkov states and plane waves exhibit periodic boundary conditions, in principle one may adjust the **k** values used in order to vary the effective simulation space. Also a CAP may be added to any of the methods and acts as an additional boundary condition. Time propagation technique is listed by terms occurring in the time propagation operator.

Method	Basis	Boundary Condition	Asymptotic Solution for ionized states	Time Propagation
Volkov basis propagation	Volkov states	periodic	correct Volkov states	V(t) only
plane wave basis propagation	plane waves	periodic	no continuation	full H(t)
FD	grid	0 at boundary	CAP	full H(t)
mask	grid and Volkov	periodic	correct Volkov states	full H(t) inside analytic outside

By left-multiplying by $\phi_{\mathbf{j}}(\mathbf{r},t)$ and integrating, this may be rewritten in a TDSE-like form as

$$i\dot{\mathbf{c}}(t) = \mathbf{V}(t)\mathbf{c}(t), \tag{11}$$

where

$$\mathbf{c}(t) = (c_{\mathbf{k}_1}(t), c_{\mathbf{k}_2}(t), ..., c_{\mathbf{k}_N}(t)) \tag{12}$$

and the matrix elements of $\mathbf{V}$ are defined as

$$\mathbf{V}_{\mathbf{kj}} = \langle \phi^V_{\mathbf{k}}(t)|V(t)|\phi^V_{\mathbf{j}}(t)\rangle. \tag{13}$$

This result indicates that by using a time-dependent Volkov state basis, one may avoid explicit propagation of H^V matrix elements as contributions from this term are handled analytically. Similarly, by accounting for the time-dependent Volkov phase present in our choice of basis, we are able to analytically describe time-dependent contributions associated with the H^V term. This splitting is somewhat similar to the interaction picture where the state vectors are propagated by the interaction free Hamiltonian and the time evolution of states is governed by the interaction.

Due to the form of the Volkov states, matrix elements may be easily calculated by multiplying well-known plane wave basis matrix elements by the Volkov phase difference

$$\mathbf{V}_{\mathbf{kj}}(t) = \langle \mathbf{k}|V(t)|\mathbf{j}\rangle e^{i(\Phi^{\mathbf{k}} - \Phi^{\mathbf{j}})}, \tag{14}$$

where we have employed the notation $\langle \mathbf{r}|\mathbf{k}\rangle = e^{i\mathbf{k}\cdot\mathbf{r}}$. If the system of interest is initialized at $t = 0$ in the absence of an external field, the Volkov phase may be taken as zero. In this case one may initialize the system by use of any popular plane wave basis method. Once initialized, plane wave matrix elements may be easily modified at each time step for use within Volkov state basis propagation (see appendix A for plane-wave formalism).

C. Time propagation

Equation (11) can be solved by discrete time step time propagation in the same way as in conventional TDSE calculations. By choosing a sufficiently short time step, Δt, during which the changes of the potential $V(t)$ and basis functions $\phi_{\mathbf{k}}(\mathbf{r},t)$ are negligibly small, we may integrate Eq. (11) to obtain

$$\mathbf{c}(t+\Delta t) = \mathrm{e}^{-i\mathbf{V}(t)\Delta t}\mathbf{c}(t). \tag{15}$$

One may numerically approximate this exponential operator by use of popular techniques such as Taylor expansion [37] or the Crank–Nicholson method [38]. In such procedures, the expansion coefficients are successively time propagated until reaching some t_{final}. Alternatively, one may iteratively solve Eq. (11) using efficient approaches developed for first-order linear differential equations such as Runge–Kutta [39].

It is often advantageous for computational implementation to rewrite Eq. (15) in the form

$$c_{\mathbf{k}}(t+\Delta t) = \sum_{\mathbf{j}} e^{i\Phi^{\mathbf{k}}(t)} \left[e^{-i\mathbf{V}^{\mathrm{PW}}\Delta t}\right]_{\mathbf{kj}} e^{-i\Phi^{\mathbf{j}}(t)} c_{\mathbf{j}}(t), \tag{16}$$

where $\mathbf{V}^{\mathrm{PW}}_{\mathbf{kj}} = \langle \mathbf{k}|V(t)|\mathbf{j}\rangle$ (see appendix B). Furthermore, in this form, one may observe that the left-most factor of $e^{i\Phi^{\mathbf{k}}(t)}$ in Eq. (16) may be combined with the right-most factor in the following time step's time propagator, $e^{-i\Phi^{\mathbf{k}}(t+\Delta t)}$,

$$e^{i\Phi^{\mathbf{k}}(t+\Delta t)} e^{i\Phi^{\mathbf{k}}(t)} = \exp\left[-i\int_t^{t+\Delta t} T^{\mathbf{k}}_{\mathbf{A}}(\tau)d\tau\right], \tag{17}$$

where $T^{\mathbf{k}}_{\mathbf{A}}(t) \equiv (\mathbf{k}+\mathbf{A}(t))^2/2$ has been introduced for the sake of concise notation. This integral may be approximated using the trapezoidal rule, allowing one to represent $\mathbf{A}(t)$ using the same time grid as the potential and wave function

$$e^{i\Phi^{\mathbf{k}}(t+\Delta t)} e^{i\Phi^{\mathbf{k}}(t)} \approx e^{-iT^{\mathbf{k}}_{\mathbf{A}}(t+\Delta t)\Delta t/2} e^{-iT^{\mathbf{k}}_{\mathbf{A}}(t)\Delta t/2}. \tag{18}$$

By relegating these individual factors back to their respective time propagators and making this approximation for each time step, one finds that this form is, in

fact, a manifestation of the split operator method

$$c_{\mathbf{k}}(t+\Delta t) = \sum_{\mathbf{k}} e^{-iT_{\mathbf{A}}^{\mathbf{k}}\Delta t/2}\left[e^{-i\mathbf{V}^{\mathrm{PW}}\Delta t}\right]_{\mathbf{kj}} e^{-iT_{\mathbf{A}}^{\mathbf{j}}\Delta t/2} c_{\mathbf{j}}(t), \quad (19)$$

with the vector potential applied in the velocity gauge [40].

The split operator method has been shown to be an efficient way to propagate the TDSE [36] and has been used in numerous applications using grid-based and pseudospectral methods [41–51], though to the authors' knowledge no previous applications utilized a splitting of the kinetic energy and the the time dependent vector potential terms. Applications in the literature typically split the potential terms in the exponential rather than kinetic due to the fact that the kinetic exponential factor, again with the vector potential excluded, is time-independent. In the current application, both the kinetic and potential factors are time-dependent. For cases where the vector potential changes more rapidly than the remaining potential terms, the split operator shown in Eq. (19) is the proper choice as it better represents the time propagation associated with that term, or, in an alternative point of view, better represents the Volkov phase factors.

D. The mask method

Within the mask method formalism, the system is divided into two regions. The partitioning $\psi_i(\mathbf{r}) = \psi_{\mathbf{A},i}(\mathbf{r}) + \psi_{\mathbf{B},i}(\mathbf{r})$ is enforced by

$$\begin{cases} \psi_{A,i}(\mathbf{r},t) = M(\mathbf{r})\psi_i(\mathbf{r},t) \\ \psi_{B,i}(\mathbf{r},t) = [1-M(\mathbf{r})]\psi_i(\mathbf{r},t) \end{cases} \quad (20)$$

where $M(\mathbf{r})$ is a mask function that smoothly connects the two regions. In region (A) the time evolution is performed with the full Hamiltonian. In Region (B) the electron-nuclear and electron-electron interactions are neglected, and, thus, the wave function may be projected into momentum space via a fast Fourier transform (FFT) and propagated analytically using the velocity gauge Volkov expansion. Another advantage of the mask method is that the mask function does not need to be enforced at every time step, this mask time step is usually defined $h = n\Delta t$. The time propagation for the full wave function proceeds as follows.

1. Propagate the real-space component $\psi_A(\mathbf{r},t)$ by applying the time evolution operator (or another method) to time $t+h$
2. Propagate the momentum space component $\xi_B(\mathbf{k},t) = \mathcal{F}\{\psi_B(\mathbf{r},t)\}$ by applying the Volkov propagator to time $t+h$
3. Reverse Fourier transform $\xi_B(\mathbf{k},t+h)$ into $\psi_B(\mathbf{r},t+h)$ and convert to the length gauge
4. Enforce the mask function to mix regions A and B.
5. Convert back to the velocity gauge and Fourier transform $\psi_B(\mathbf{r},t+h)$ to momentum space $\xi_B(\mathbf{k},t+h)$
6. Repeat steps 1–5 until time t_{final} is reached

The analytic propagation of ψ_B allows for very large simulation domains (over 3000 Bohr have been used) due to the favorable $NlogN$ scaling from FFT routines. The only approximation employed in this formalism is that the electron does not experience the Coulomb potential; however, for masking regions associated with ψ_B which are far from any nuclei, this is a reasonable approximation. It should be noted, that in principle one can use Coulomb-Volkov wave functions to eliminate this approximation [52, 53]. In this paper, the mask function is defined to be

$$M(\mathbf{r}) = \begin{cases} 1, & \text{if } r < R_C \\ 1-\sin^2(\frac{\pi}{2}\frac{r-R_C}{R_A-R_C}), & \text{if } R_C \leqslant r \leqslant R_A \\ 0, & \text{if } r > R_A \end{cases} \quad (21)$$

as used in ref. [30]. Because the real-space wave function in region B is known at times when the mask function is enforced, a position based mask can also be used to prevent artificial wrapping of the wave function into the opposing side of the simulation box.

Since the mask method utilizes a two-part wave function, and these parts are not orthogonal to each other, care must be taken when calculating densities and other properties, as noted in Ref [30]. The mixing of the two regions occurs, in principle, at a different frequency than the time propagation in the FD region. This can introduce spurious artifacts within the high harmonic spectra and other properties if only ψ_A is used. Therefore, time-dependent properties should only be calculated using the full wave function.

III. ONE DIMENSIONAL TEST CALCULATIONS WITH SOFT COULOMB POTENTIAL

Findings are reported below for simulations of one electron bound to a soft Coulomb potential, given as [9]

$$V(a,Q;x) = -\frac{Q^2}{(a^2+x^2)^{1/2}}, \quad (22)$$

where a has been set to unity. This electron is subject to a laser represented as a variation of the smooth turn-on pulse [25],

$$f(n) = \begin{cases} E_0 \sin(\dfrac{\pi t}{2T_c})\sin(\omega t), & \text{if } 0 \leq t \leq T_c, \\ E_0 \sin(\omega t), & \text{otherwise.} \end{cases} \quad (23)$$

In each calculation parameters $E_0 = 0.1$, $\omega = 0.148$, and $T_c = 6/\omega$ have been used. These simulations have been carried out within a computational box of width 400 Bohr and time propagated using a fourth-order Taylor expansion of the exponential time propagator (Eq. (15) for Volkov states and using the full Hamiltonian for the other methods). Results using various bases are compared to one another as well as FD calculation benchmarks. Because of the large box size, no CAPs were used unless otherwise stated. Finally, the functionality of the mask method is analyzed, discussed, and compared to the use of CAPs.

A. Convergence with respect to basis dimension

Final densities, $\rho(x) = |\psi(x, t_{\text{final}})|^2$, resulting from the ionization process are presented in Fig. 1 for various choices of basis and basis dimension, with a time step of 0.02 a.u. used for each method. The densities produced by the Volkov state basis converge quickly with respect to the number of basis functions, with the 201 basis function density (∼1 function for every 2 Bohr) nearly matching that of the converged solution. For the case of the plane wave basis, however, the density produced using 201 functions does not agree well with the converged solution, and, furthermore, even when using 301 basis functions spurious oscillations appear. It is likely a combination of the additional flexibility from the Volkov states' time-dependence and the fact that these states are constructed as interaction-free analytic solutions to field influence which allows them to better represent the time-dependent wave function.

While the FD method results in unreasonably large grid spacings when using fewer basis functions, represented as grid points, the results for such cases are shown in order to illustrate by comparison the advantage of Volkov states and plane waves. As continuous functions, these bases may accurately represent the wave function by means of a smaller basis dimension. For each method, the density appears well converged with 1551 basis functions within the 400 Bohr box used for the simulation. The agreement of the converged solutions is presented in Fig. 2. Furthermore, the harmonic spectra from these simulations are shown in Fig. 3. When enough basis functions are used, all methods converge to the same result.

Key when simulating electron dynamics under the effects of intense lasers is achieving an accurate rate of ionization, since this will affect the energy levels, harmonics, fragmentation, ionization potential, etc. Therefore, ensuring that the basis is able to accurately represent the ionization of system is an important consideration. The total ionization probability is defined as

$$P_{\text{ion}}(t) = 1 - \sum_{n,\text{bound}} |\langle \phi_n(x) | \psi(x,t) \rangle|^2, \qquad (24)$$

where $\phi_n(x)$ are the eigenfunctions of the Hamiltonian at

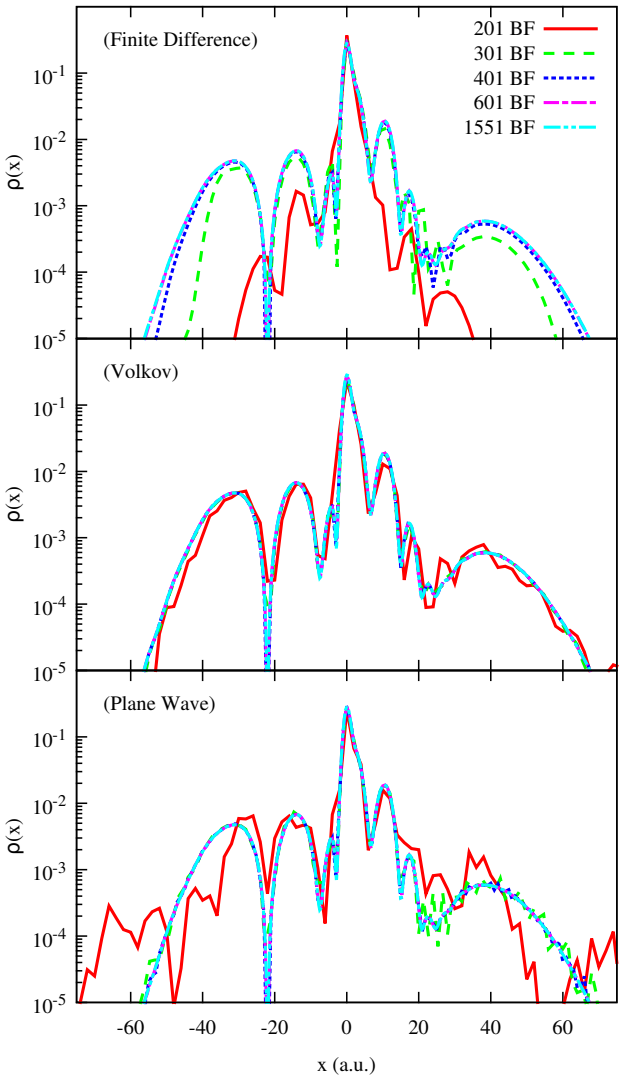

FIG. 1. The density at $t_{\text{final}} = 80$ a.u. using (top) FD, (middle) Volkov states, and (bottom) plane waves for various choices of basis dimension.

$t = 0$ and the sum is performed over those states which are determined to be bound, i.e. correspond to negative energy levels. Comparison of the calculated total ionization probabilities resulting from the various methods shows that the Volkov basis and the plane wave basis both converge with ≈ 300 basis functions, as shown in Fig. 4. The plane wave basis seems to give similar results as the Volkov basis for fewer basis functions with one performing better at some times and the other better at other times. The FD method seems to require a finer basis in order to converge, though gives the same result as the other bases when using a sufficient number of basis functions.

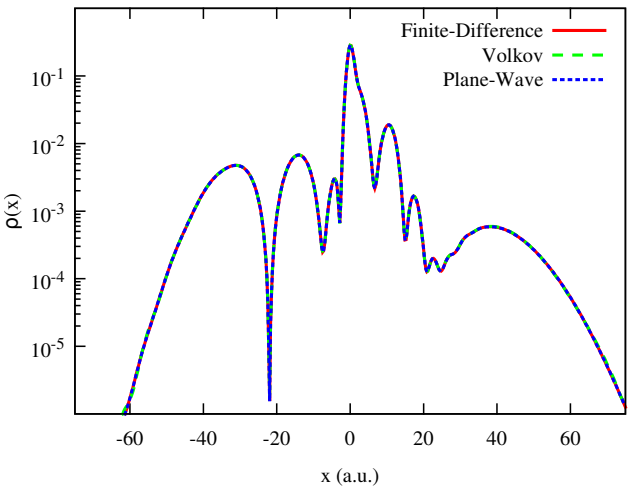

FIG. 2. Density at $t_{\text{final}} = 80$ a.u. for several choices of basis, each employing 1551 basis functions.

B. Convergence with respect to time step

The various representations were compared using an assortment of time step sizes. The Volkov basis is shown in Fig. 5 to outperform all other choices by an order of magnitude with respect to the length of time step allowed, with a norm, $\langle\psi(t)|\psi(t)\rangle$, which is preserved for time steps as long as 0.4 a.u. The other methods are significantly less stable near their maximum time step and their norms deviate suddenly and rapidly during the time propagation. As recorded in table II, the maximum stable time step observed for the other methods is 0.04 a.u. for FD and mask methods and 0.02 for the plane wave bases. For large time step sizes, the norm as calculated using the Volkov basis representation deviates from unity; however, this deviation does not result in dramatic divergence of the wave function as with the other methods used. In fact, the final densities of these large time step Volkov simulations remain quite faithful to the converged solution but with noise on the order of 10^3. The energies of the Volkov and FD simulations match perfectly for short time steps and begin to deviate at the same time step at which the norm deviates from unity, as shown in Fig. 6.

TABLE II. Maximum time step sizes allowed for various methods. Fourth-order Taylor time propagation used for all except in the case of DFT using the Volkov basis in which the split operator approach was employed.

Method	SC Δt_{max} (a.u.)	DFT Δt_{max} (a.u.)
FD	0.04	0.04
Mask	0.04	0.04
Plane wave basis	0.02	NA
Volkov basis	0.40	0.12

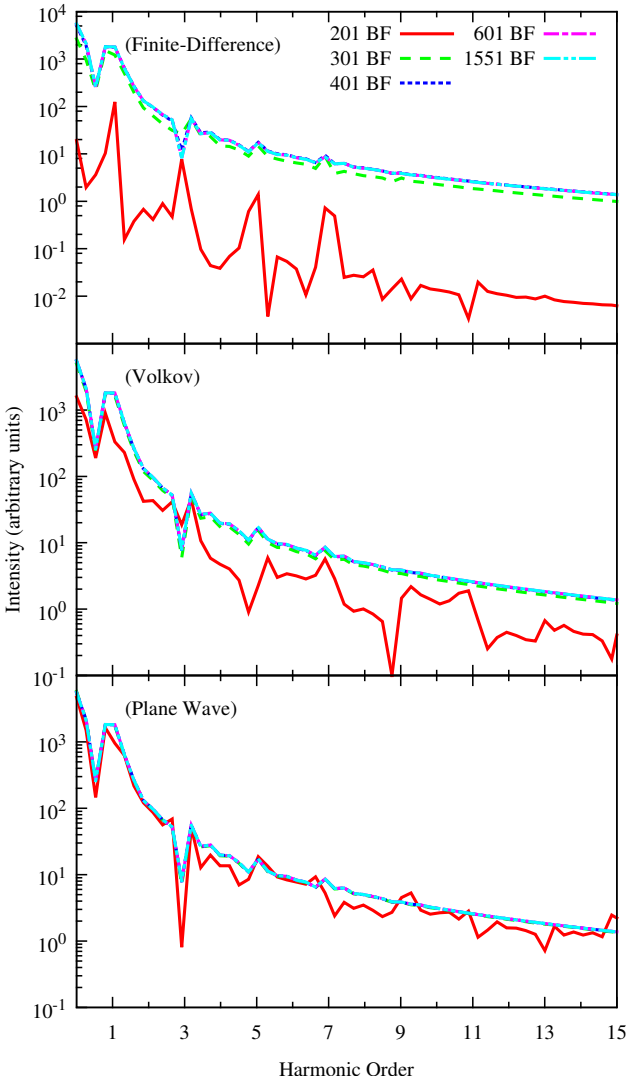

FIG. 3. Harmonic spectra generated using (top) FD, (middle) Volkov states, and (bottom) plane waves and time propagated until $t_{\text{final}} = 160$ a.u. The number of basis functions is shown.

C. Split operator and Volkov methods

As shown in Eq. (19), the long known split operator method is in fact a form of the Volkov method. However the propagation using a Volkov state basis can provide a more accurate representation for the influence of the vector potential if a finer time grid is used for integrating the Volkov phase factors. The differences between the densities of Volkov basis and the split operator method at $t = 80$ a.u. are shown in Fig. 7 in both linear and log scales, where the Volkov phase factor was integrated on a 100 times smaller time step. It can be seen that this more accurate representation of the Volkov phase factors allows for a final density which better agrees with that of the converged solution.

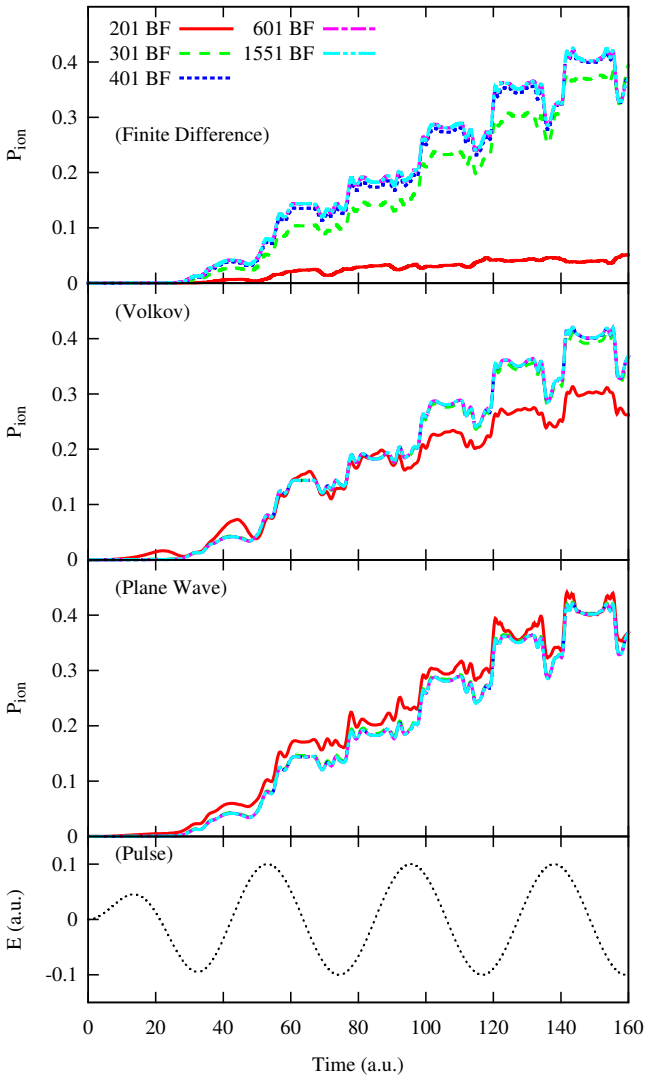

FIG. 4. Ionization probability using (top) FD, (middle) Volkov states, and (bottom) plane waves. The number of basis functions is shown.

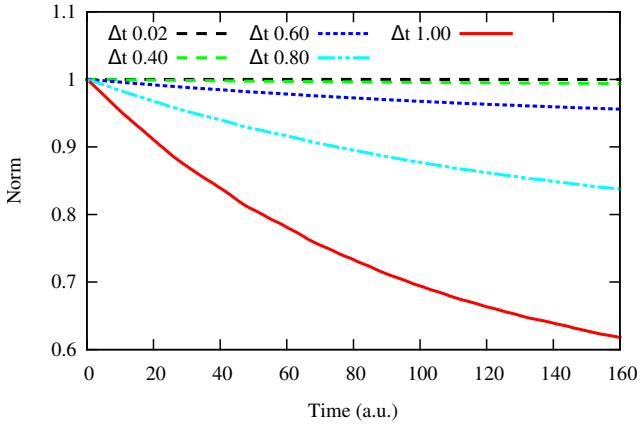

FIG. 5. The norm of the Volkov wave function as a function of time for various time step sizes using the Volkov basis propagation method. In each case 1551 basis functions were used.

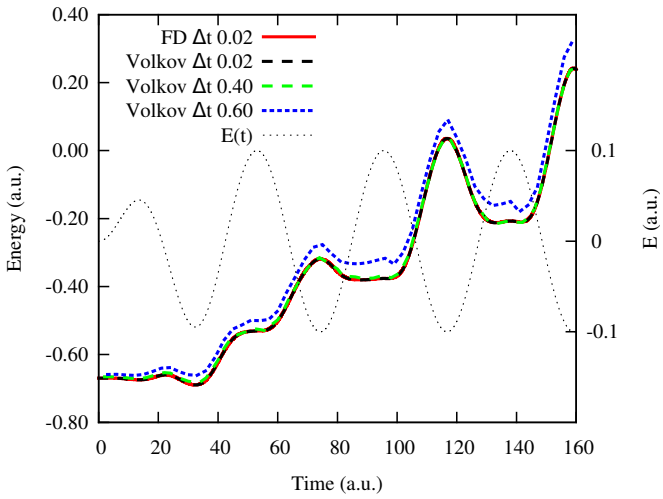

FIG. 6. Time-dependent energy for various choices of time step size using the Volkov basis time propagation method. FD time propagation method has also been presented for $\Delta t = 0.02$.

D. Mask method in 1D

The mask method presents a simple method to cheaply expand the size of the simulation domain by making the approximation that far from any nuclei the particle-particle interaction is much weaker than the interaction with the laser. For strong fields and moderate distances, this approximation becomes appropriate. If only the laser-particle interactions are kept, then time propagation is analytic in that region using the Volkov propagator. Therefore, the mask method is a combination of a region of the Volkov state basis and another region, which may use a different basis.

To determine how sensitive the mask method is to the closeness of the mask function distance, R_C, 1-D simulations were performed with different values of R_C. The time propagated density is presented in Fig. 8 for one electron subject to a soft Coulomb potential and a laser of the form described in Eq. (23). With a masking region as close as 40 Bohr, the density matches nearly exactly with the full FD solution; in fact, the resulting density for $R_C = 20$ Bohr agrees quite well despite some small inconsistencies. The density of the $R_C = 10$ Bohr shows some deviations from the full FD calculation but still contains information of the rescattered wave function, or recollison in the case of multiple electrons, that would be lacking if a CAP were used. Since the Volkov and FD methods produce equivalent results, as presented above, a comparison between the mask method and Volkov method is not shown.

The ionization probability, Eq. (24), as calculated us-

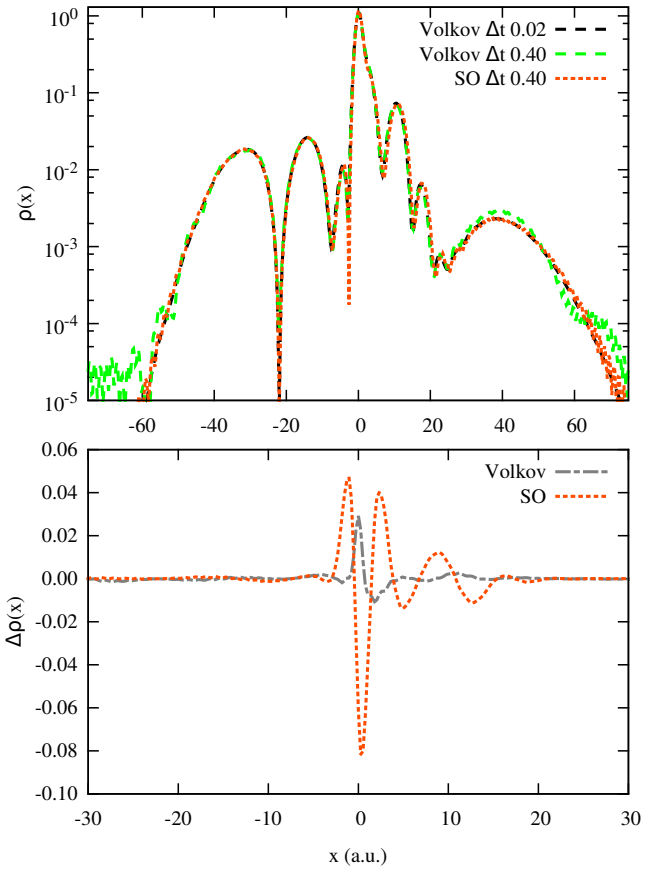

FIG. 7. (Top) The densities at $t_{\text{final}} = 80$ a.u. using both Volkov and split operator (labeled SO) propagation and (bottom) the density differences for each method using $\Delta t = 0.4$ compared with the Volkov basis propagation result for $\Delta t = 0.02$ which is considered to be the converged solution. Note that both log and linear scales are used.

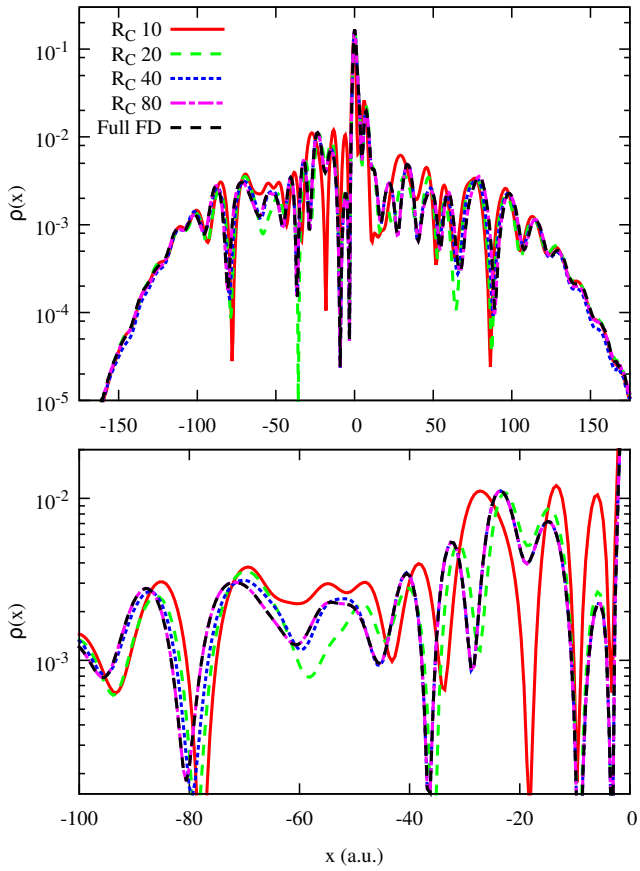

FIG. 8. Density a $t_{\text{final}} = 160$ calculated using the mask method for various distances of R_C, with $R_A = R_C + 10$. Top and bottom graphs are the same data presented using different scales.

ing the mask method with various distances is shown in Fig. 9. For $R_C = 20$ Bohr, the solution is reasonably converged to that of the full FD representation. The same simulation is also presented using CAPs of the form developed by Manolopoulos [54]

$$-iw(x) = \frac{-i}{2}\left(\frac{2\pi}{\Delta x}\right)^2 f(y), \tag{25}$$

$$f(y) = 4/c^2\left(\frac{1}{(1+y)^2} + \frac{1}{(1+y)^2} - 2\right), \tag{26}$$

$$y = \frac{(x - x_1)}{\Delta x}. \tag{27}$$

Here x_1 is the start of the absorbing region, x_2 is the simulation boundary, $\Delta x = x_2 - x_1$, c is a constant set to 2.62. In order to maintain numerical stability when representing this potential on a grid, it is necessary to modify Δx as $\Delta x' = x_2 - x_1 + \gamma$, where γ is approximately 1 grid spacing.

By using CAPs, one is able to remove the reflections from the boundary, however all the information from that part of the wave function is lost as indicated by the too high rate of ionization, also shown in Fig. 9. As the CAP is placed further from the SC potential the ionization more closely resembles the larger box. However as the simulation proceeds even the CAP staring at 80 Bohr begins to deviate at $t = 150$ a.u. The mask method has a distinct advantage in the convergence with distance of the fully propagated wave function.

It should be noted, that in principle any method can be used to time propagate the inner region. A real space grid using FD has been used in these calculations, but other bases such as Gaussian basis functions, plane waves, or Volkov states would also be valid. Also the grid points in real space are chosen to match between the inner and outer regions, though this too is not a requirement. In principle the wave function in the outer region could be described using a subset of the full Volkov states resulting in reduced computational effort.

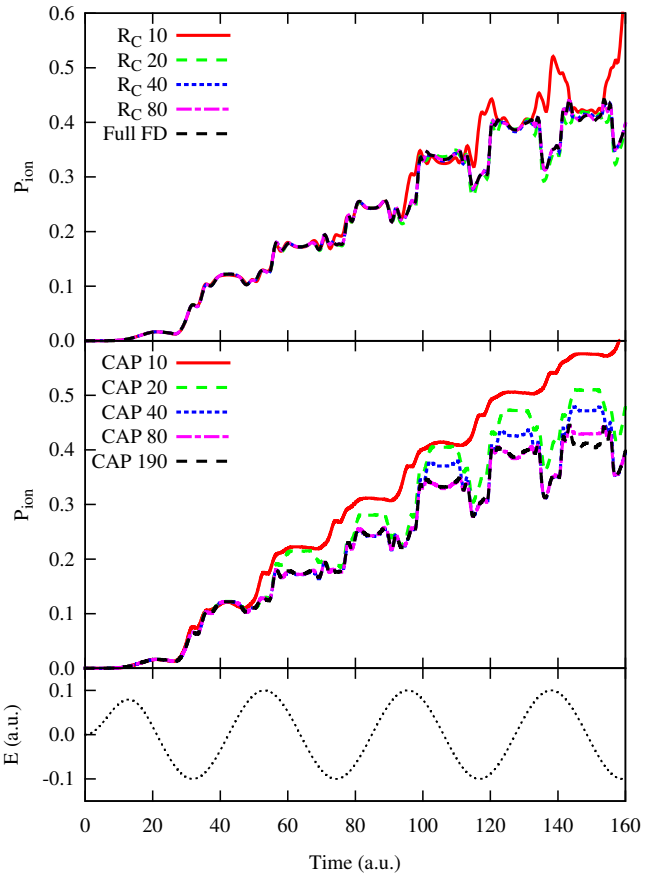

FIG. 9. The ionization probability (Top) The mask method and (Bottom) FD with CAP.

IV. EXTENSION TO PERIODIC CASES

The Volkov basis treatment may be similarly applied to systems subject to periodic potentials, for which they are well suited due to their periodicity. In such cases, the wave function is known to take on the form of a Bloch state

$$\psi(\mathbf{r},t) = e^{i\mathbf{K}\cdot\mathbf{r}} u_{\mathbf{K}}(\mathbf{r},t), \tag{28}$$

where the function $u_{\mathbf{K}}(\mathbf{r})$ has the same periodicity as the potential. In this case one may make use of modified velocity gauge Volkov states

$$\tilde{\phi}_{\mathbf{k},\mathbf{K}}(\mathbf{r},t) = e^{\mathbf{k}\cdot\mathbf{r}} e^{-i\Phi^{\mathbf{k}+\mathbf{K}}}. \tag{29}$$

Here, the basis is **K**-dependent. This choice is attributed to the advantageous property

$$i\frac{\partial}{\partial t}\left[e^{\mathbf{K}\cdot\mathbf{r}}\tilde{\phi}_{\mathbf{k},\mathbf{K}}(\mathbf{r},t)\right] = H^V\left[e^{\mathbf{K}\cdot\mathbf{r}}\tilde{\phi}_{\mathbf{k},\mathbf{K}}(\mathbf{r},t)\right] \tag{30}$$

which allows one to expand $u_{\mathbf{K}}(\mathbf{r})$ into these modified Volkov states in the same manner as that employed in sec. II B.

By substituting Eq. (28) into the TDSE and using the expansion

$$u_{\mathbf{K}}(\mathbf{r},t) = \sum_{\mathbf{k}} c_{\mathbf{k},\mathbf{K}}\tilde{\phi}_{\mathbf{k},\mathbf{K}}(\mathbf{r},t), \tag{31}$$

one is able to obtain an equation of the same form as eq. (11) governing the time evolution of the expansion coefficients

$$i\dot{\mathbf{c}}(t) = \mathbf{V}(\mathbf{K},t)\mathbf{c}(t). \tag{32}$$

In this case the matrix elements are **K**-dependent and again may be expressed in terms of plane wave matrix elements multiplied by a Volkov phase difference

$$\mathbf{V}_{\mathbf{kj}} = \langle\mathbf{k}|V(t)|\mathbf{j}\rangle e^{i(\Phi^{\mathbf{k}+\mathbf{K}}-\Phi^{\mathbf{j}+\mathbf{K}})}. \tag{33}$$

As in the finite case, a plane wave basis may be used to initialize the system. Then the matrix elements associated with H^V need only be modified by the Volkov phase factor.

This representation is expected to be particularly suited for the studying of laser-induced electronic phenomena such as high harmonic generation (HHG) in solids which has recently been introduced as a topic of much interest[55, 56]. We present an example calculation of HHG for one electron in a periodic 1D Mathieu potential

$$V(x) = -V_0[1+\cos(2\pi x/L)], \tag{34}$$

where the parameters V_0 and L are the potential amplitude set as 0.37 Hartree and the length of the unit cell set as 8 Bohr, respectively. The system is subject to a laser field of the form presented in Eq. (23).

Similar calculations have been recently carried out using basis splines [57] as well as Bloch and Houston bases [58]. The latter is another example of time-dependent basis functions as it is comprised of instantaneous eigenstates of the Hamiltonian[59, 60]. The Houston states are calculated by diagonalizing the velocity gauge Hamiltonian for each time step, and, in the present formalism, the wave function expanded in these states is equivalent to the plane wave solution at any point in time. The Houston state basis has become very popular for the calculation of HHG within crystals [57, 61, 62] because, in that representation, the intraband and interband contributions can be separated and explicitly studied.

In the following discussion, the HHG spectrum is obtained by taking the Fourier transform of the cell-averaged probability current, $\frac{1}{L}\int_0^L \mathbf{j}(x)dx$. Resulting HHG spectra are displayed in Fig. 10. One calculation describes $u_{\mathbf{K}}(\mathbf{r})$ as an expansion in plane waves while the other employs the described Volkov basis propagation. Both have been time propagated by repeatedly applying the exponential time propagation operator described in Eq. (15) via the Crank–Nicholson approximation.

For small time steps, the two calculations agree and their HHG spectra overlap. However, due to the fact

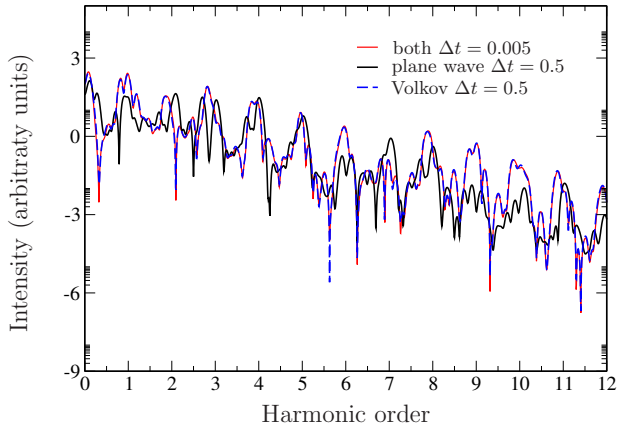

FIG. 10. Calculations of the HHG spectra of one electron in a periodic Mathieu potential using both plane wave and Volkov bases. This calculation was performed using a single **K**-point and propagated until $t_{\text{final}} = 500$. Laser parameters $E_0 = 0.1$ and $\omega = 0.148$ were used.

that the Volkov expansion coefficients vary much more slowly than those of the plane wave basis, for larger time steps the Volkov basis description remains accurate to the converged spectrum, while the plane wave description noticeably diverges. The advantage of the Volkov basis is quite noticeable in the density at $t_{\text{final}} = 500$ a.u., depicted in Fig. 11. For smaller time steps, the two solutions overlap. However, in the case of large time steps, the Volkov basis representation well resembles the converged, small time step density, whereas the plane wave representation diverges significantly. These results suggests that by propagating periodic systems using a Volkov basis, one might be allowed larger time step sizes and thus significantly improved computational speeds.

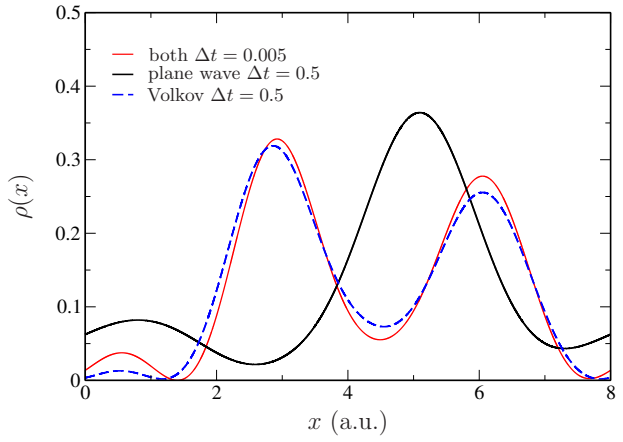

FIG. 11. Electron density at $t_{\text{final}} = 500$ for time step sizes of $\Delta t = 0.005$ and $\Delta t = 0.5$. The potential and laser parameters were the same as those used in Fig. 10.

V. APPLICATION IN TIME-DEPENDENT DENSITY FUNCTIONAL THEORY

Time-dependent density functional theory (TDDFT) [63] is one of the most promising tools used to study the interaction of laser pulses with atoms and molecules [50, 64–66]. TDDFT has been proven to produce accurate descriptions of the total and individual ionization yields for Ne and Ar atoms exposed to strong laser pulses [64] and has also helped to explain the enhanced ionization in molecules as well as the energetics and dynamics of laser-assisted field evaporation [67]. Above threshold ionization HHG has also been a subject of TDDFT studies [66, 68–70].

For the case of TDDFT applied to a laser field perturbation, one is tasked with solving the time-dependent Kohn–Sham equation (TDKS),

$$i\frac{\partial \phi_k(\mathbf{r},t)}{\partial t} = \left[\frac{1}{2}\left(-i\nabla + \mathbf{A}\right)^2 + V_{\text{KS}}\right]\phi_k(\mathbf{r},t), \qquad (35)$$

where ϕ_k represent fictitious non-interacting single particle orbitals which yield the same density as the true electron wave function. Note that, as in Eq. (2), the laser field have been incorporated within the Hamiltonian via the velocity gauge.

The Kohn–Sham potential, V_{KS}, may be decomposed as

$$V_{\text{KS}} = V_{\text{H}}[\rho](\mathbf{r},t) + V_{\text{XC}}[\rho](\mathbf{r},t) + V_{\text{ion}}(\mathbf{r},t). \qquad (36)$$

Here ρ is the electron density, which is defined by a sum over all occupied orbitals:

$$\rho(\mathbf{r},t) = \sum_{k=1}^{\infty} N_k |\psi_k(\mathbf{r},t)|^2, \qquad (37)$$

where the coefficient N_k accounts for the number of electrons in each orbital.V_{H} is the Hartree potential, defined by

$$V_{\text{H}}(\mathbf{r},t) = \int d\mathbf{r}' \frac{\rho(\mathbf{r}',t)}{|\mathbf{r}-\mathbf{r}'|}, \qquad (38)$$

which accounts for the electrostatic Coulomb interactions between electrons. V_{XC} is the exchange-correlation potential, whose exact form is unknown, and V_{ion} is the external potential due to the ions. The potential of the ions can be represented by employing pseudopotentials centered at each ion, for example the norm-conserving pseudopotentials of the form given by Troullier and Martins [71]. These pseudopotentials may also have nonlocal terms, which will be effected by the choice of gauge. In the case of an external field which is changing more rapidly than V_{KS}, the Volkov basis is expected to be optimal, yielding similar advantages as when solving the TDSE.

TDDFT calculations have been performed for the ionization of He using both Taylor time propagation on a

real-space grid and using the Volkov basis, implemented in split operator fashion. The simulation was conducted within a $87 \times 56 \times 56$ Bohr cubic box with grid spacings of 0.53 Bohr in each dimension, with the laser polarized along the long axis (x-axis). The exchange-correlation potential was approximated using the adiabatic local–density approximation with the parameterization of Perdew and Zunger [72]. A CAP of the form given in Eqs. (25) and (26) was placed in all directions starting at ± 19 Bohr and extending to the boundary. Because the simulation box is much smaller for the 3D system, the number of bound states are reduced by the confinement. Therefore the ionization was calculated by integrating the number of electrons that remained in the box using,

$$N(t) = \int_V \rho(\mathbf{r}, t) d^3x. \tag{39}$$

Also because of the smaller box size, a laser pulse with a Gaussian envelope was used, the form of which is given as,

$$\mathbf{E}(t) = E_{max} \exp\left[-\frac{(t-t_0)^2}{2a^2}\right] \hat{\mathbf{k}} \sin(\omega t). \tag{40}$$

A peak field strengths of $E_0 = 0.1$ and $E_0 = 1$ a.u. were used with $a = 58$ giving a pulse duration of 97 a.u. and a pulse was centered at $t = 200$ a.u.

The resulting time-dependent densities matched between the Volkov basis and FD simulations with an external field of $E_0 = 0.1$ a.u., as proof that the Volkov basis is applicable to 3D systems and the DFT method. Furthermore the Volkov TDDFT simulations were able to use a larger time step by a factor of 3. When $E_0 = 1$ a.u. peak field was used, there was a distinct breakdown of the CAP in the FD simulations, causing the wave function to bounce off of the boundaries of the simulation box. The problems with the FD simulations in strong fields were not seen in the Volkov method, which ionized steadily to zero, as shown in Fig. 12. The FD simulations in a strong field even perform worse if a much smaller time step is used. While the reason for the failure of the CAP in FD simulations is not understood, the Volkov method does not suffer from this flaw.

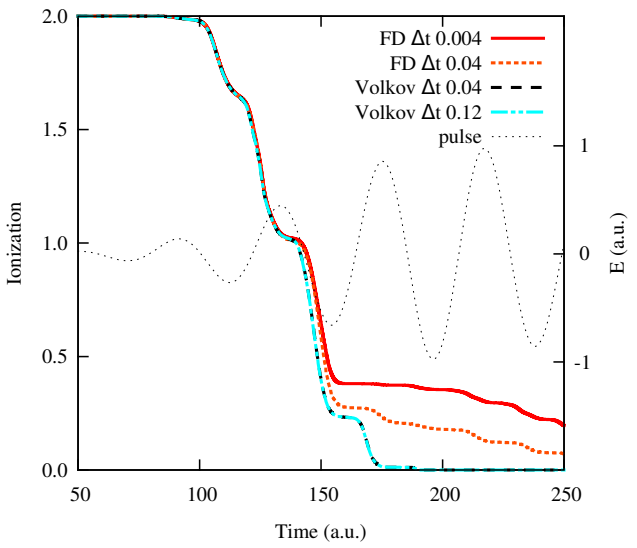

FIG. 12. Comparison of the ionization between FD and Volkov simulations on He (laser pulse peak field 1 a.u. frequency 0.46 a.u.).

VI. SUMMARY

We have demonstrated that calculations solving the Schrödinger equation for strong laser-induced electron dynamics under the influence of an an arbitrary potential may be well represented on a basis comprised of time-dependent Volkov states, as shown by agreement to results obtained using well-established benchmark bases. Furthermore, the Volkov basis has been shown to provide improved accuracy compared to representations using alternative popular choices such as the real-space grid or plane wave basis. The improved accuracy is the result of expansion coefficients which evolve on a significantly larger time-scale. This advantage may be alternatively capitalized upon in the form of larger computational time steps and thus faster computer program run-times.

The mask method, a wave function splitting technique that combines FD method with asymptotic Volkov state representation, was also tested. The time-dependent wave function was found to converge quickly with respect to masking distances, with that of 20–30 Bohr yielding excellent results. These distances are far improved over those required for the CAP separations. The mask method allows for high accuracy, by extending the simulation domain when describing laser-induced phenomena.

The Volkov basis representation has been implemented in 1D periodic calculations as well as 3D time-dependent density functional theory and has exhibited similar improvements in each of these cases. We believe that this choice of basis may improve calculations concerning the interaction of laser fields and matter at the quantum scale such as in the case of high harmonic generation. Alternately the Volkov method may allow for more efficient time propagation of the TDSE which in turn allows for the simulation of longer lived phenomena and larger systems.

In the present work for the Volkov states we have used a plane wave basis set which is mapped to a finite difference grid to facilitate the calculation of the potential matrix elements with FFT. This renders the Volkov states to be periodic in the simulation cell. This restriction can be easily removed by adding extra Volkov states with plane waves spanning larger cells. One may also use atomic orbitals, e.g. Gaussian basis functions to represent the electron orbitals and add Volkov states to describe the ionization. In this dual basis approach the Volkov states

are not tied to any grid and can represent the wave function in as large computational region as required for the desired accuracy. These possibilities will be pursued in future works.

VII. ACKNOWLEDGMENT

This work has been supported by the National Science Foundation (NSF) under grants No. Phy 1314463 and No. IIA126117.

Appendix A: Plane Wave Basis

The following is supplementary information to the material in sec. II for the plane wave basis. Plane waves can be used to emulate a basis set using a generalized approach. The wave function is represented as a linear combination of expansion coefficients and basis functions

$$\Psi(x,t) = \sum_k b_k(t)\phi_k(x). \tag{A1}$$

In this case the basis functions ϕ_k are described by plane waves

$$\phi_k(x) = e^{ikx}. \tag{A2}$$

We would like to solve the TDSE for the case of an electron under the influence of a time-dependent potential $V(x,t)$

$$i\frac{\partial}{\partial t}\Psi(x,t) = \left[-\frac{1}{2}\frac{\partial^2}{\partial x^2} + V(x)\right]\Psi(x,t). \tag{A3}$$

By substituting the plane wave basis into the TDSE and evaluating the derivatives, one arrives at

$$i\sum_k \dot{b}_k\phi_k = \frac{1}{2}\sum_k b_k k^2\phi_k + \sum_k b_k V\phi_k. \tag{A4}$$

One may then arrive at the characteristic coefficient differential equation by left-multiplying by $\phi_k^*(x)$ and integrating over real-space

$$\dot{b}_k = \frac{1}{2}k^2 b_k + \sum_{k\prime} V_{kk\prime}b_{k\prime}, \tag{A5}$$

where $V_{kk\prime} \equiv \langle k|V(t)|k'\rangle$. This equation may be solved using the methods discussed in sec. II C.

Appendix B: Decomposition of Volkov Matrix exponential

The following is a proof for the rearrangement of Eq. (16) from sec. II. One may relate the potential matrix in the Volkov basis, $\mathbf{V}^{\mathrm{v}}(t)$, to that in the plane wave basis. This relationship is key to the connection of the Volkov method and the split operator approach. Using Eq. (14) as

$$\mathbf{V}^{\mathrm{v}}(t) = \mathbf{F}^{-1}(t)\mathbf{V}^{\mathrm{pw}}(t)\mathbf{F}(t), \tag{B1}$$

where $F_{jk}(t) \equiv \delta_{jk}e^{-i\Phi^k(t)}$ are the Volkov phase factors, these phase factors may be separated from the full exponential, allowing one to rewrite the expression in Eq. (15) as

$$e^{-i\mathbf{V}^{\mathrm{v}}(t)\Delta t} = \mathbf{F}^{-1}(t)e^{-i\mathbf{V}^{\mathrm{pw}}(t)\Delta t}\mathbf{F}(t). \tag{B2}$$

This is shown in the following proof.

For an arbitrary $N \times N$ diagonalizable matrix $\mathbf{A}$, one may define the characteristic eigenvalues λ and eigenvectors $\mathbf{y}$ using the equation

$$\mathbf{A}\mathbf{y} = \lambda\mathbf{y}. \tag{B3}$$

The eigenvector matrix $\mathbf{Y}$ may then be defined as the matrix whose columns are the eigenvectors $\mathbf{y}_1, \mathbf{y}_2, ..., \mathbf{y}_N$. The matrix $\mathbf{A}$ can be then be decomposed as $\mathbf{A} = \mathbf{Y}^{-1}\mathbf{\Lambda}\mathbf{Y}$, where $\Lambda_{ij} = \delta_{ij}\lambda_i$. We now define a matrix $\hat{\mathbf{A}}$ who shares eigenvalues with $\mathbf{A}$ and whose eigenvector matrix is $\mathbf{X} = \mathbf{F}\mathbf{Y}$, where $F_{ij} = \delta_{ij}F_i$ and F_i defines the elements of some arbitrary vector. The matrix $\hat{\mathbf{A}}$ may then be decomposed as

$$\hat{\mathbf{A}} = \mathbf{X}^{-1}\Lambda\mathbf{X} = \mathbf{F}^{-1}\mathbf{Y}^{-1}\Lambda\mathbf{Y}\mathbf{F}, \tag{B4}$$

and the matrix exponential may be thus decomposed as

$$e^{a\hat{\mathbf{A}}} = \mathbf{X}^{-1}e^{a\Lambda}\mathbf{X} = \mathbf{F}^{-1}\mathbf{Y}^{-1}e^{a\Lambda}\mathbf{Y}\mathbf{F} = \mathbf{F}^{-1}e^{a\mathbf{A}}\mathbf{F}. \tag{B5}$$

[1] W. Kaiser and C. G. B. Garrett, Phys. Rev. Lett. **7**, 229 (1961).
[2] H. B. Bebb and A. Gold, Phys. Rev. **143**, 1 (1966).
[3] J. E. Bayfield and P. M. Koch, Phys. Rev. Lett. **33**, 258 (1974).
[4] M. Gavrila, *Atoms in Intense Laser Fields* (Academic Press Inc, United States, 1992).
[5] K. Burnett, V. Reed, and P. Knight, J. Phys. B: At., Mol. Opt. Phys. **26**, 561 (1993).
[6] P. B. Corkum, Phys. Rev. Lett. **71**, 1994 (1993).
[7] M. Protopapas, C. H. Keitel, and P. L. Knight, Rep. Prog. Phys. **60**, 389 (1997).
[8] X. Zhou and C. Lin, Phys. Rev. A **61**, 053411 (2000).
[9] Q. Su and J. Eberly, Phys. Rev. A **44**, 5997 (1991).
[10] S. Chelkowski, C. Foisy, and A. D. Bandrauk, Phys. Rev. A **57**, 1176 (1998).

[11] K. Varga, Phys. Rev. E **85**, 016705 (2012).
[12] K. Schafer, B. Yang, L. DiMauro, and K. Kulander, Phys. Rev. Lett. **70**, 1599 (1993).
[13] A. D. Bandrauk, *Molecules in Laser Fields* (CRC Press, 1993).
[14] M. Schultze, M. Fieß, N. Karpowicz, J. Gagnon, M. Korbman, M. Hofstetter, S. Neppl, A. L. Cavalieri, Y. Komninos, T. Mercouris, C. A. Nicolaides, R. Pazourek, S. Nagele, J. Feist, J. Burgdörfer, A. M. Azzeer, R. Ernstorfer, R. Kienberger, U. Kleineberg, E. Goulielmakis, F. Krausz, and V. S. Yakovlev, Science **328**, 1658 (2010).
[15] C. I. Blaga, F. Catoire, P. Colosimo, G. G. Paulus, H. G. Muller, P. Agostini, and L. F. DiMauro, Nat. Phys. **5**, 335 (2009).
[16] D. Shafir, H. Soifer, B. D. Bruner, M. Dagan, Y. Mairesse, S. Patchkovskii, M. Y. Ivanov, O. Smirnova, and N. Dudovich, Nature **485**, 343 (2012).
[17] A. N. Pfeiffer, C. Cirelli, M. Smolarski, D. Dimitrovski, M. Abu-samha, L. B. Madsen, and U. Keller, Nat. Phys. **8**, 76 (2012).
[18] L. Torlina, F. Morales, J. Kaushal, I. Ivanov, A. Kheifets, A. Zielinski, A. Scrinzi, H. G. Muller, S. Sukiasyan, M. Ivanov, and O. Smirnova, Nat. Phys. **11**, 503 (2015).
[19] L. Keldysh, J. Exptl. Theoret. Phys. **Vol: 20**, 1307 (1965).
[20] F. H. M. Faisal, J. Phys. B: Atom. Molec. Phys. **6**, L89 (1973).
[21] D. B. Milošević, Phys. Rev. A **74**, 063404 (2006).
[22] H. R. Reiss, Phys. Rev. A **22**, 1786 (1980).
[23] J. L. Krause, K. J. Schafer, and K. C. Kulander, Phys. Rev. Lett. **68**, 3535 (1992).
[24] V. Reed and K. Burnett, Phys. Rev. A **43**, 6217 (1991).
[25] K. Varga and J. A. Driscoll, *Computational Nanoscience* (Cambridge University Press, England, 2011).
[26] R. Kosloff and D. Kosloff, J. Comput. Phys. **63**, 363 (1986).
[27] U. Riss and H.-D. Meyer, J. Phys. B: At., Mol. Opt. Phys. **26**, 4503 (1993).
[28] S. Chelkowski and A. D. Bandrauk, Int. J. Quantum Chem. **60**, 1685 (1996).
[29] D. Varsano, M. Marques, and A. Rubio, Comput. Mater. Sci. **30**, 110 (2004).
[30] U. De Giovannini, D. Varsano, M. A. Marques, H. Appel, E. K. Gross, and A. Rubio, Phys. Rev. A **85**, 062515 (2012).
[31] D. Volkov, Z. Phys. **94**, 250 (1935).
[32] L. Collins and A. Merts, J. Opt. Soc. Am. B **7**, 647 (1990).
[33] L. A. Collins and A. L. Merts, Phys. Rev. A **40**, 4127 (1989).
[34] H. Miyagi and L. B. Madsen, Phys. Rev. A **93**, 033420 (2016).
[35] A. Russakoff, Y. Li, S. He, and K. Varga, J. Chem. Phys. **144**, 204125 (2016).
[36] T. R. Taha and M. I. Ablowitz, J. Comput. Phys. **55**, 203 (1984).
[37] A. Askar and A. S. Cakmak, J. Chem. Phys **68**, 2794 (1978).
[38] J. Crank and P. Nicolson, Adv. Comput. Math. **6**, 207 (1996).
[39] R. LeVeque, *Finite Difference Methods for Ordinary and Partial Differential Equations* (Society for Industrial and Applied Mathematics, 2007).
[40] M. Feit, J. Fleck, and A. Steiger, J. Comput. Phys. **47**, 412 (1982).
[41] A. D. Bandrauk and H. Shen, J. Chem. Phys. **99**, 1185 (1993).
[42] P. Bader, S. Blanes, and F. Casas, J. Chem. Phys. **139**, 124117 (2013).
[43] T. Seideman, M. Y. Ivanov, and P. B. Corkum, Phys. Rev. Lett. **75**, 2819 (1995).
[44] M. R. Hermann and J. A. Fleck, Phys. Rev. A **38**, 6000 (1988).
[45] X.-M. Tong and S.-I. Chu, Chemical Physics **217**, 119 (1997).
[46] R.-F. Lu, P.-Y. Zhang, and K.-L. Han, Phys. Rev. E **77**, 066701 (2008).
[47] P.-L. He, N. Takemoto, and F. He, Phys. Rev. A **91**, 063413 (2015).
[48] J. P. Hansen, T. Sørevik, and L. B. Madsen, Phys. Rev. A **68**, 031401 (2003).
[49] X.-M. Tong, T. Watanabe, D. Kato, and S. Ohtani, Phys. Rev. A **64**, 022711 (2001).
[50] X.-M. Tong, G. Wachter, S. A. Sato, C. Lemell, K. Yabana, and J. Burgdörfer, Phys. Rev. A **92**, 043422 (2015).
[51] D. Bauer and P. Koval, Computer Physics Communications **174**, 396 (2006).
[52] H. R. Reiss and V. P. Krainov, Phys. Rev. A **50**, R910 (1994).
[53] D. G. Arbó, J. E. Miraglia, M. S. Gravielle, K. Schiessl, E. Persson, and J. Burgdörfer, Phys. Rev. A **77**, 013401 (2008).
[54] D. E. Manolopoulos, J. Chem. Phys. **117**, 9552 (2002).
[55] J. P. Marangos, Nat. Phys. **7**, 97 (2011).
[56] S. Ghimire, A. D. DiChiara, E. Sistrunk, P. Agostini, L. F. DiMauro, and D. A. Reis, Nat. Phys. **7**, 138 (2011).
[57] Z. Guan, X.-X. Zhou, and X.-B. Bian, Phys. Rev. A **93**, 033852 (2016).
[58] M. Wu, S. Ghimire, D. A. Reis, K. J. Schafer, and M. B. Gaarde, Phys. Rev. A **91**, 043839 (2015).
[59] W. V. Houston, Phys. Rev. **57**, 184 (1940).
[60] J. B. Krieger and G. J. Iafrate, Phys. Rev. B **33**, 5494 (1986).
[61] M. S. Wismer, S. Y. Kruchinin, M. Ciappina, M. I. Stockman, and V. S. Yakovlev, Phys. Rev. Lett. **116**, 197401 (2016).
[62] G. Vampa, C. R. McDonald, G. Orlando, D. D. Klug, P. B. Corkum, and T. Brabec, Phys. Rev. Lett. **113**, 073901 (2014).
[63] E. Runge and E. K. U. Gross, Phys. Rev. Lett. **52**, 997 (1984).
[64] A. Crawford-Uranga, U. De Giovannini, E. Räsänen, M. J. T. Oliveira, D. J. Mowbray, G. M. Nikolopoulos, E. T. Karamatskos, D. Markellos, P. Lambropoulos, S. Kurth, and A. Rubio, Phys. Rev. A **90**, 033412 (2014).
[65] A. Russakoff, S. Bubin, X. Xie, S. Erattupuzha, M. Kitzler, and K. Varga, Phys. Rev. A **91**, 023422 (2015).
[66] A. Russakoff and K. Varga, Phys. Rev. A **92**, 053413 (2015).
[67] E. P. Silaeva, K. Uchida, Y. Suzuki, and K. Watanabe, Phys. Rev. B **92**, 155401 (2015).
[68] X. Chu and G. C. Groenenboom, Phys. Rev. A **93**, 013422 (2016).
[69] A. Castro, A. Rubio, and E. K. U. Gross, Eur. Phys. J. B **88**, 191 (2015).
[70] E. P. Fowe and A. D. Bandrauk, Phys. Rev. A **81**, 023411 (2010).

[71] N. Troullier and J. L. Martins, Phys. Rev. B **43**, 1993 (1991).

[72] J. P. Perdew and A. Zunger, Phys. Rev. B **23**, 5048 (1981).